Multiple-Beam Fizeau Fringe-Pattern Analysis Using Fourier Transform Method for Accurate Measurement of Fiber Refractive Index Profile of Polymer Fiber

M. A. EL-MORSY,[1] T. YATAGAI,[1] A. HAMZA,[2] M. A. MABROUK,[3] T. Z. N. SOKKAR[2]

[1] Institute of Applied Physics, Yatagai Laboratory, University of Tsukuba, Tsukuba, Ibaraki 305-5873, Japan

[2] Physics Department, University of Mansoura, Mansoura, Egypt

[3] Physics Department, Damietta, University of Mansoura, Damietta, Egypt

Received 30 March 2001; accepted 16 June 2001

ABSTRACT: In this article the Fourier transform method is applied to analyze multiple-beam interference Fizeau fringes. The real part of the inverse Fourier transform is used to estimate a theoretical pattern. This pattern coincides with the experimental one. A derivative-sign binary image of the interference pattern is also used in automated determination of the contour line of the fringe pattern, regardless of the quality of this pattern. A correlation between the pixel size and the accuracy of the measured fiber refractive index is presented. © 2002 Wiley Periodicals, Inc. J Appl Polym Sci 85: 475–484, 2002

Key words: multiple-beam Fizeau fringes; refractive index profile; polyethylene fiber; fringe analysis; Fourier transform

INTRODUCTION

The study of the optical properties of fibers is a valuable task in fiber research because their structural characteristics are manifested in their optical properties. There are many parameters that affect the characteristics of optical fibers, such as the fiber radius, refractive index profile, numerical aperture, material dispersion, and attenuation. The refractive index profile and material dispersion have strong affects on the group delay characteristics of an optical fiber.[1] The values of the refractive indices of textile fibers, using plane polarized monochromatic light vibrating parallel and perpendicular to the fiber axis, give useful information about the molecular arrangement of these fibers. They can also provide information about the structural and mechanical properties of these fibers. Thus, refractive index measurements using accurate methods have been studied by numerous authors.[2–9]

Different techniques have been developed to determine the fiber refractive index profile. All of these techniques have their own advantages and disadvantages. The ideal measuring technique should be nondestructive and applicable to any preform and have high accuracy, high resolution, and easy measurement and processing of data.[10]

The multiple-beam Fizeau fringe system is a sensitive optical technique, and it needs no special sample preparation for measuring the refractive index profile of textile and optical fibers.[2,7,8,11] Interference fringes are formed across the fiber when immersed in a silvered liquid

Correspondence to: M. A. El-Morsey (elmorsy@optlab2.bk.tsukuba.ac.jp or elmorsym@yahoo.com).

Journal of Applied Polymer Science, Vol. 85, 475–484 (2002)

wedge interferometer illuminated by a parallel beam of monochromatic light. The shift in the position of the interference fringe is formed because the fiber inside the interferometer works as a phase object. The value of this shift depends on the optical properties of the fiber. It gives quantitative information about the optical properties of the fiber under test and its structure. The methods in which matching immersion liquids are used give good results for the fiber refractive index profiles, especially when liquid and fiber cladding both have refractive indices close to each other. However, to minimize the error in the measured data, it is essential to take into consideration the effect of refraction of the beam through the liquid–fiber and core–cladding interfaces.[4,7,12] The manual work for processing multiple-beam Fizeau fringes is however time consuming, cumbersome, and error prone because the interferogram must be photographed, enlarged to a suitable magnification, and the measured quantities then obtained from the magnified image.

Automated, high-speed image-processing techniques are used to analyze the fringe pattern and give an accurate analysis. The main procedure in automatic fringe-pattern analysis is fringe skeleton extraction. Several investigators[13–19] proposed various digital image-processing algorithms for extracting fringe skeletons from the fringe patterns. This process can be classified into two categories. In the first category the fringe field is identified as a binary image and the fringe skeletons are obtained using algorithms that were primarily developed for optical character recognition. A recently published article[8] comes under this category. In the second category the intensity variation within a fringe is used in devising algorithms for fringe skeleton determination. The algorithm applied by Yatagai et al.[13] comes under this category.

One of the biggest problems involved in practical digital fringe-pattern analysis is the noise reduction problem, regardless of what type of image-processing method is used. Without noise the fringe-pattern analysis is much easier to analyze and is usually straightforward. Unfortunately, during the acquisition and digitization of the fringe pattern various noises appear in the digital fringe patterns. We applied a Fourier transform (FT) passband filter to reduce the pattern's noise.

The main focus in this work is to analyze the multiple-beam Fizeau fringe pattern using 1-dimensional (1-D) FT for accurate measurement of the refractive index profile of a polyethylene polymer fiber.

THEORETICAL

Refractive Index Profile

Interference methods are used to determine the refractive index distribution along the fiber radius from the lateral shift of the interference fringe, which gives the phase shift of light passing through it. The fiber cross section is assumed to be divided into N circular zones. For a large number of layers, each layer can be considered to have a constant refractive index. The interference fringe shift (Z_Q) of the Qth layer in the fiber region is related to the refractive index (n_Q) of the layer as

$$\begin{aligned}\frac{\lambda Z_Q}{2h} = \sum_{j=1}^{Q-1} 2n_j \Bigg\{ & \sqrt{(R-(j-1)a)^2 - \left(\frac{d_Q n_o}{n_j}\right)^2} \\ & - \sqrt{(R-ja)^2 - \left(\frac{d_Q n_o}{n_j}\right)} \Bigg\} \\ & + 2n_Q \sqrt{(R-(Q-1)a)^2 - \left(\frac{d_Q n_o}{n_j}\right)^2} \\ & - n_o\{\sqrt{R^2 - d_Q^2} + \sqrt{R^2 - X_Q^2}\} \qquad (1)\end{aligned}$$

where λ is the wavelength of the light used, h is the interfering space, R is the fiber radius, a is the layer thickness ($a = R/N$), $n_o = n_L$ is the immersion liquid refractive index, and X_Q and d_Q are the emergent and incident ray distances from the fiber center, respectively, where

$$\begin{aligned} d_Q &= \frac{n_Q\left(R - \left(Q - \frac{1}{2}\right)a\right)}{n_o} \\ X_Q &= R\,\sin(\beta_Q) \\ \beta_Q &= 2\sum_{j=0}^{Q-1}(\alpha_j - \theta_j) + \theta_0 \qquad (2)\end{aligned}$$

where β is the angle between the radius at the ray exit point and the incident ray and θ and α are the incidence and refraction angle, respectively.[7] Using eq. (1) and the Z_Q value a computer program was prepared to measure the refractive index pro-

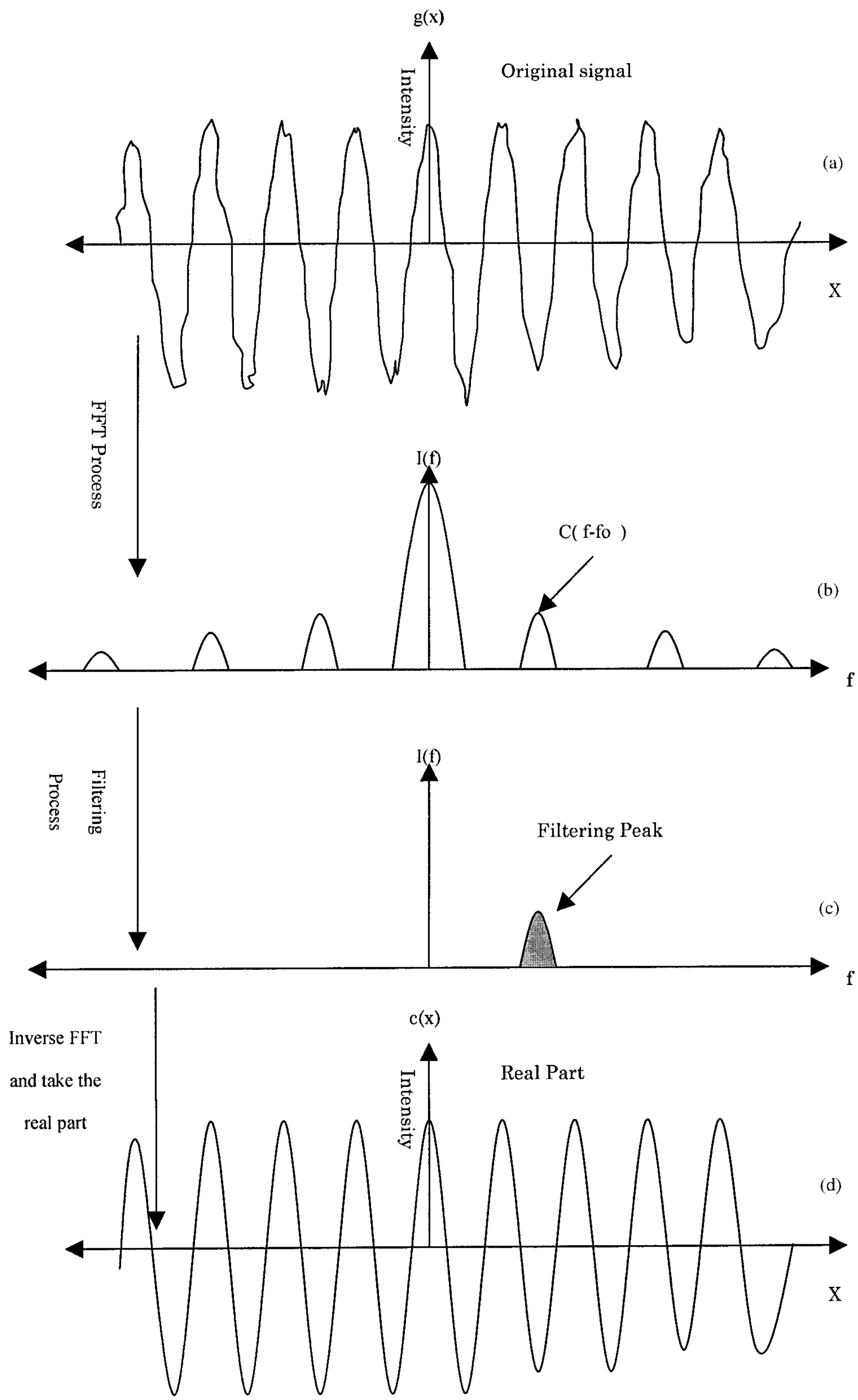

Figure 1 A schematic diagram of 1-dimensional (1-D) filtering: (a) the original 1-D relatively noise-free fringe pattern, (b) the modulus of the Fourier transform of the original, (c) filtering of the desired peak of the former, and (d) the real part of the inverse Fourier transform.

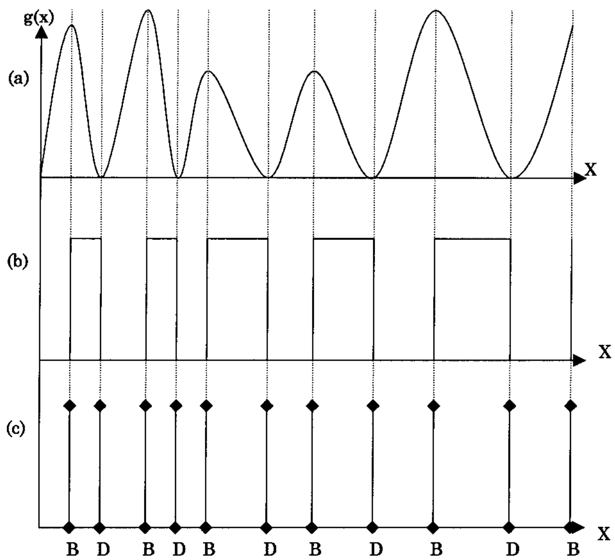

Figure 2 A schematic diagram of a derivative-sign binary fringe pattern: (a) the intensity distribution of the interference fringe pattern, (b) the intensity distribution of the derivative-sign binary fringe pattern of the former, and (c) the fringe skeleton; B, bright; D, dark.

file of the fibers. The accuracy of this profile depends on the accuracy of the fringe shift measurement. The following section deals with the methods of fringe shift data refinement.

Fourier Filtering

Interference periodic fringe and their Fourier spectra occur quite frequently in optics. The FT method of fringe-pattern analysis is useful in removing the noise from the fringe pattern. Fourier fringe analysis was originally introduced and demonstrated by Takeda et al.[20,21] The technique was also studied by many others.[22–25] The intensity data contained in such a fringe pattern can be written as

$$g(x) = a(x) + b(x)\cos(2\pi f_0 x + \phi(x)) \qquad (3)$$

where $a(x)$ represents the background variations, $b(x)$ describes variations in the fringe visibility, $\phi(x)$ is the phase of the object, and f_0 is the carrier frequency. This equation can be rewritten as

$$g(x) = a(x) + c(x)\exp(i2\pi f_0 x) + c^*(x)\exp(-i2\pi f_0 x) \qquad (4)$$

where

$$c(x) = \tfrac{1}{2}\, b(x)\exp(i\phi(x))$$

and $c^*(x)$ denotes complex conjugation of $c(x)$.

Using the FT algorithm, we compute the 1-D FT of eq. (4) for the variable x as shown in Figure 1 and y is fixed.

$$G(f) = A(f) + C(f - f_0) + C^*(-\mathrm{f}-\mathrm{f}_0) \qquad (5)$$

where the capital letters denote Fourier spectra, f is the variable in spatial frequency space, and $C(f - f_0)$ is the FT of $c(x)$ with respect to x. From eq. (5) one can notice that $a(x)$, $b(x)$, and $\phi(x)$ are slowly varying functions compared to the variations introduced by the f_0. Thus, when the FT of the fringe pattern is taken, three peaks are obtained as shown in Figure 1. The FT of the term $A(f)$ is placed in the center of the spectrum and the FTs of $C(f - f_0)$ and $C^*(f - f_0)$ will be symmetric with respect to the center and placed at a distance that is determined by f_0.[26,27] We make use of either of the two peaks' spectra on the carrier, say $C(f - f_0)$. In other words, the unwanted peaks are filtered out in this step. Using the inverse FT (IFT), if we compute the IFT of $C(f - f_0)$ with respect to f, then the term $c(x)$ itself will be obtained. The real part of $c(x)$ represents the filtered image pattern.

Image Skeleton (Fringe Centers)

The location of the geometric fringe centers can be determined by two methods. The first method uses a thinning algorithm; the disadvantage of this algorithm is that it usually requires numerous iterations in order to peel the fringe pattern. The second method consists of differential filter techniques.[18,19] This algorithm is very simple because it requires one step to find the center of the fringe pattern and is suitable for straight, circular, or any type of fringe pattern. More explanations about the differential filter techniques are given in the following text.

Regardless of how dark or bright the interference fringes are and no matter what the fringe density, one of the most characteristic of the interferometric fringe patterns is that the derivatives in the fringe normal direction on both sides of a fringe centerline have opposite signs. We used this feature to determine the derivative-sign binary image of a fringe pattern. In the binary image, if the derivative signs of the original fringe pattern of the points are positive, the points are

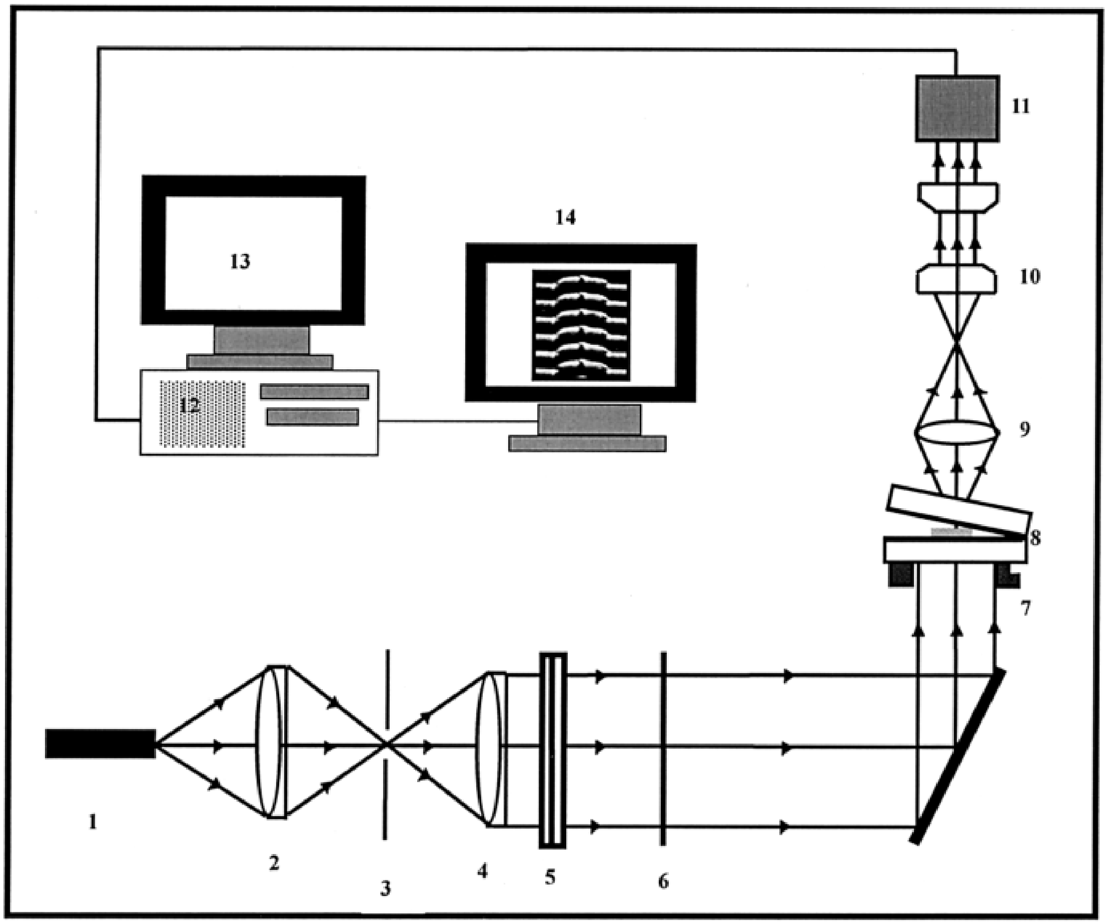

Figure 3 The optical setup for producing multiple-beam Fizeau fringes in transmission: 1, mercury lamp; 2, condenser lens; 3, iris diaphragm; 4, collimating lens; 5, polarizer; 6, monochromatic interference filter; 7, microscope stage; 8, silvered liquid wedge interferometer; 9, microscope objective; 10, microscope ocular; 11, CCD camera; 12, frame grabber; 13, graphic and text screen; 14, multisync monitor.

set to a bright value. On the other hand, if the derivative signs of the original fringe pattern of the points are negative, the points are set to a dark value, as shown in Figure 2(a,b). From this figure one can see that the boundaries of the binary fringes are exactly the centerlines of the original fringes without any deviation [Fig. 2(c)]. The derivative-sign binary fringe image is expressed as follows:

$$g(x, y) = \left\{ \begin{array}{ll} \text{bright color (say 255)} & \text{if} \quad \Delta g(x, y) > 0 \\ \text{dark color (say 0)} & \text{if} \quad \Delta g(x, y) < 0 \end{array} \right\} \tag{6}$$

where

$$\Delta g(x, y) = g(x, y) - g(x + 1, y)$$

After constructing the derivative-sign binary image pattern it is easy to extract the fringe centerlines over the image field using the following equation:

$$g(x, y) = |g(x, y) - g(x - 1, y)| \tag{7}$$

EXPERIMENTAL

A schematic diagram representing the optical setup for producing multiple-beam Fizeau fringes is shown in Figure 3. The fringes are characterized by sharp bright fringe on a dark background. This system is reported elsewhere.[9] The liquid

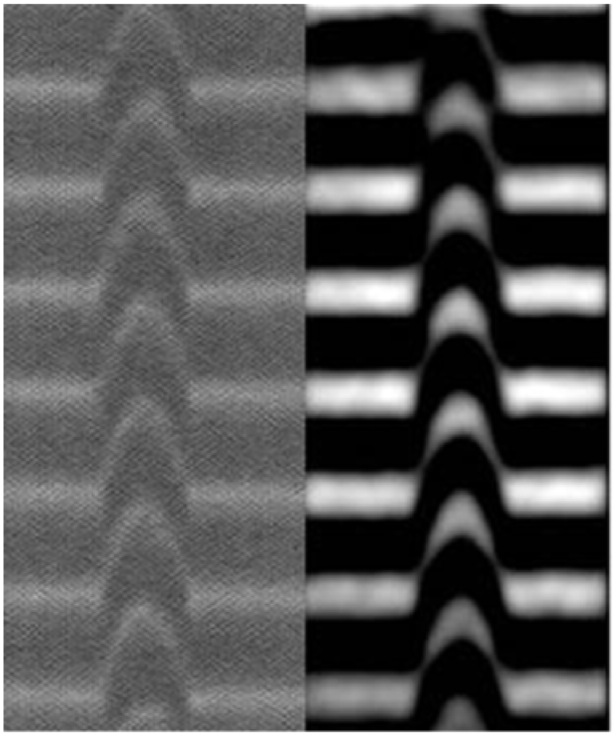

(a) (b)

Figure 4 (a) The original microinterferogram of the polyethylene fiber with a draw ratio of 7.5 using monochromatic light vibrating parallel to the fiber axis and (b) the resultant noise-free normalized fringe pattern of the original.

wedge interferometer is adjusted in such a way that the fiber is exactly perpendicular to the interference fringes in the liquid region. The accuracy of the refractive index profile, and hence the structural parameter measurements, are affected by the deviation of the fiber and fringes from a right angle. Deviation from a right angle by 1° or less causes a negligible change in the measured quantities.[5] The intensity of the multiple-beam Fizeau image is converted to an electric video signal and sampled to yield a digital picture made up of 512 × 512 sample points, each of which is quantized to 256 discrete gray levels. Using a 2-dimensional intensity sensor (Panasonic CCD microcamera attached directly to the microscope), the digital picture is stored in the memory of a digital frame grabber. The stored picture is transferred to a PC with a 500-MHz microprocessor and recorded on the mass storage device of a disk. A crosshair is used to adjust the fiber to be perpendicular to the fringes. A relay lens is inserted between the microscope and the CCD camera to sharpen the interferogram.

RESULTS AND DISCUSSION

Fringe Centerline Extraction

Two polyethylene fiber samples were used, which were drawn to different draw ratios (7.5 and 10). The draw ratio is the ratio of the fiber length after drawing to the original fiber length. Monochromatic light (λ = 546.1 nm) vibrating parallel and perpendicular to the fiber axis is used. Figure(4a) is the original multiple-beam Fizeau fringe pattern of the polyethylene fiber with a draw ratio of 7.5. We applied the FT method to remove the pattern's noise and the result is shown in Figure 4(b).

To determine the contour line we must first determine the derivative binary fringe image of the pattern by using eq. (6). Thus, by determining the edges of the derivative binary fringe image, we can determine the contour line of the original bright fringe image. Figure 5(a) is the original fringe pattern produced by using polyethylene fiber with a draw ratio of 10 and light vibrating perpendicular to the fiber axis. Figure 5(b) is the contour line plotted inside the original pattern, while Figure 5(c) shows the contour line with a dark background. Figure 6(a–c) is the same as Figure 5(a–c) but using the light vibrating parallel to the fiber axis. Also, by using the real part of the IFT we could estimate another pattern, which coincides with the experimental pattern. Figure 7(a–c) shows the experimental pattern, the estimated pattern, and the derivative binary fringe

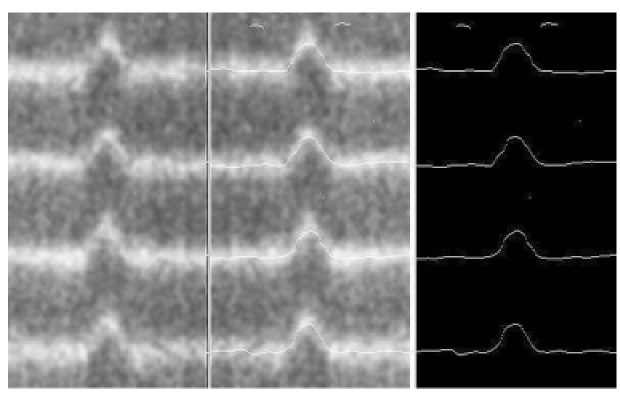

(a) (b) (c)

Figure 5 (a) A microinterferogram of the polyethylene fiber with a draw ratio of 10 using monochromatic light vibrating perpendicular to the fiber axis, (b) an extracted fringe contour line of the former shown on the background of the original pattern, and (c) the extracted fringe contour line in a dark background.

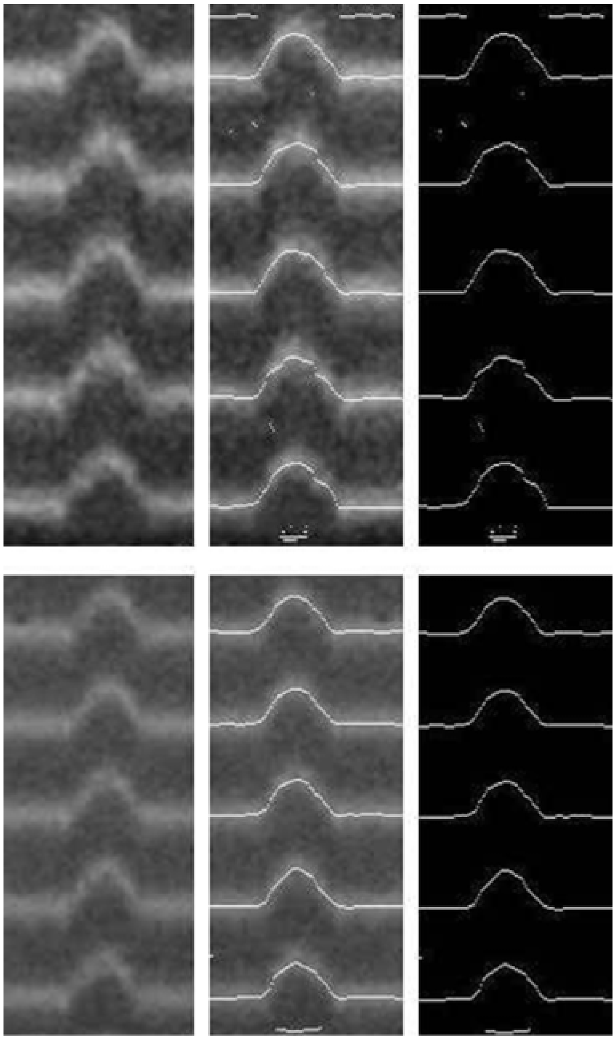

(a) (b) (c)

Figure 6 (a) A microinterferogram of the polyethylene fiber with a draw ratio of 10 using monochromatic light vibrating parallel to the fiber axis, (b) an extracted fringe contour line of the former shown on the background of the original pattern, and (c) the extracted fringe contour line in a dark background.

image of the estimated pattern. Figure 8(a) is the experimental image, Figure 8(b) is the contour line of this pattern, Figure 8(c) is the estimated pattern of Figure 8(a), and Figure 8(d) is the contour line of Figure 8(c). Observe that the contour line in Figure 8(d) is more stable than in Figure 8(b).

Refractive Index Profile Measurement

The refractive index profiles of the drawn fibers were obtained using the original and estimated patterns. The monochromatic light had a 546.1-nm wavelength. The fringe patterns shown in Figure 8(a,c) were used to obtain the refractive index profile shown in Figure 9. The refractive index profiles shown in Figure 10 were calculated from the interferogram produced using polyethylene fiber with a draw ratio of 10 and monochromatic light vibrating perpendicular to fiber axis. The immersion liquid used had a refractive index of 1.5297, and the pixel size was found to be 0.87 μm.

The pixel size plays an important role in the measurement accuracy, so the difference between the results of the methods applied in Figures 9 and 10 is due to the change in the pixel size. It is clear from Figures 9 and 10 that the refractive index profile is nearly flat. The relationship between the absolute difference in the average value of the refractive index of both methods and the pixel size is shown in Figure 11. From Figure 11 it is clear that with low pixel size there is little difference in the results of both methods, so we recommend use of this method with low pixel size. Considering the affect of the pixel size in the measurement accuracy, the microinterferogram shown in Figure 6(a, upper) has a pixel size of 0.625 μm. The refractive index profile given in Figure 12 is calculated from this microinterferogram and its estimated pattern. It is clear that there is only a small error in the measurement of the refractive index for both methods, and the two curves in Figure 12 coincide with each other and tend to be one curve.

The fringe pattern shown in Figure 7(a) is so poor that it was not possible to automatically

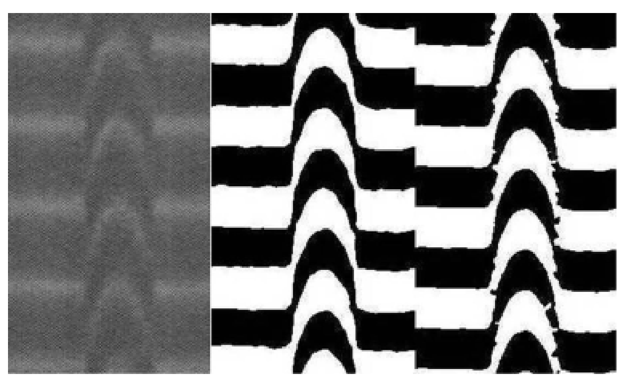

(a) (b) (c)

Figure 7 (a) The original pattern, (b) the estimated pattern produced by using the real part of the inverse Fourier transform of the original, and (c) the derivative binary fringe image of the estimated pattern.

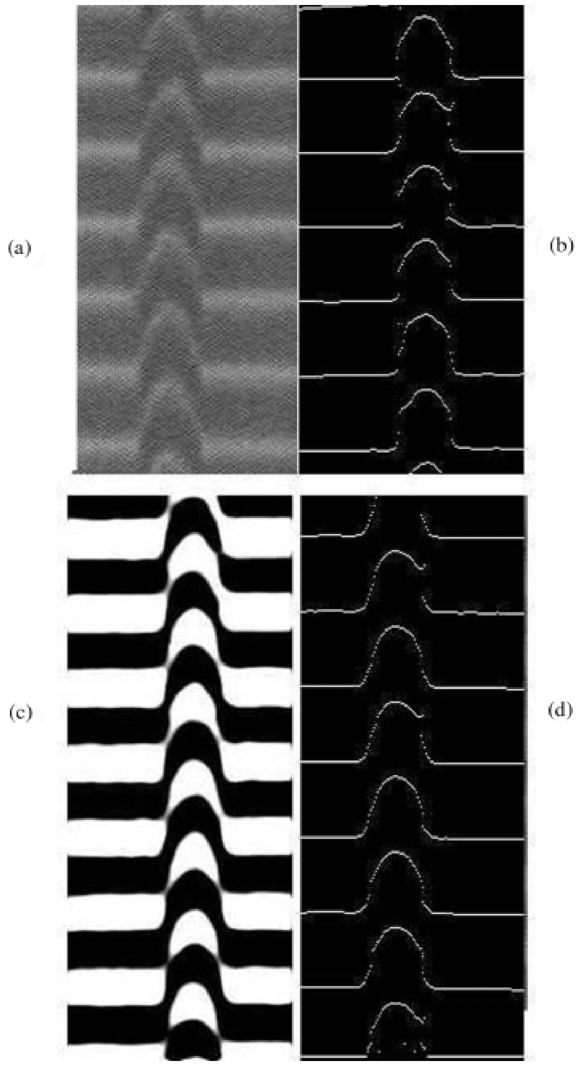

Figure 8 (a) The original pattern, (b) the contour line of the fringe pattern (original), (c) the estimated pattern produced using the real part of the inverse Fourier transform of the original, and (d) the contour line of the fringe pattern (estimated).

determine its contour line, so we manually calculated the refractive index. However, its estimated fringes were used to automatically calculate the refractive index profile as shown in Figure 13. The results show good agreement, which encourages use of the suggested method of estimated fringes to determine the refractive index profile of the fiber.

CONCLUSIONS

Compared with conventional methods, the FT method has the advantage of higher accuracy.[29] It

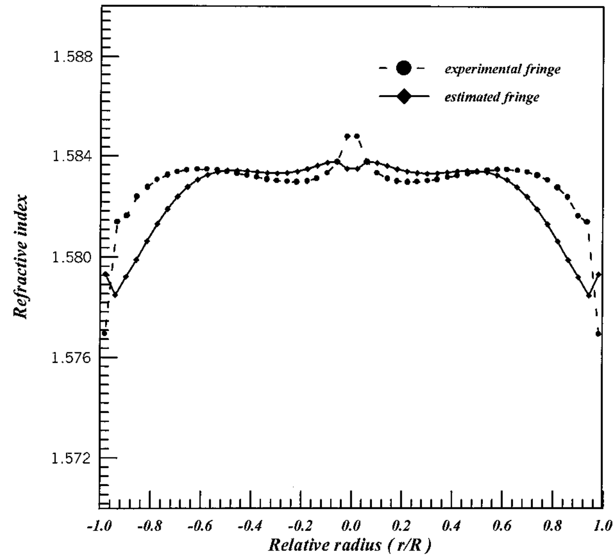

Figure 9 The refractive index profile of the polyethylene fiber with a draw ratio of 7.5 using experimental and estimated patterns. Monochromatic light vibrating parallel to the fiber axis was used. The pixel size is 1.32 μm, and the immersion liquid has a refractive index of 1.5787.

could be used to enhance and analyze multiple-beam Fizeau fringes. Fully automated determination of the contour line is possible, whatever the

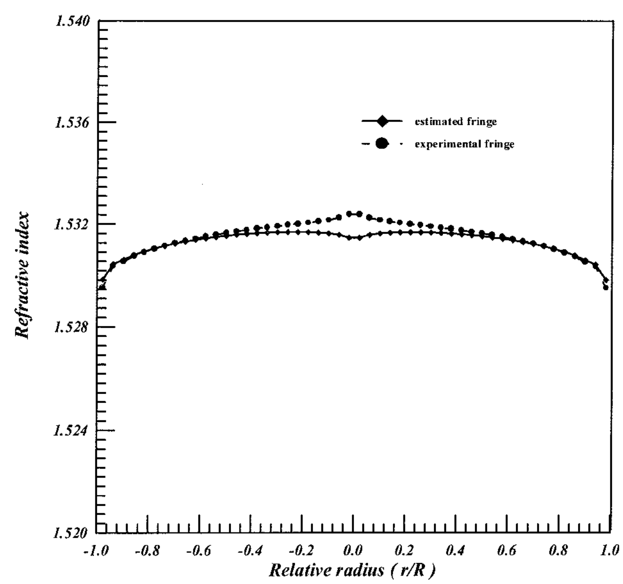

Figure 10 The refractive index profile of the polyethylene fiber with a draw ratio of 10 using experimental and estimated patterns. The monochromatic light vibrates perpendicular to the fiber axis. The pixel size is 0.87 μm, and the immersion liquid has a refractive index of 1.5297.

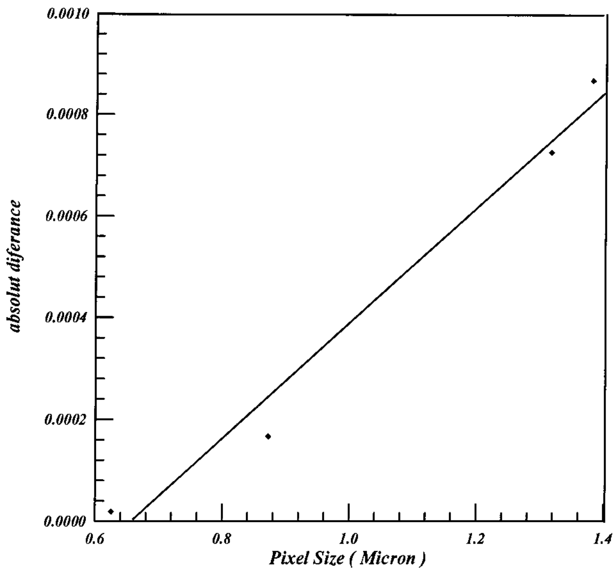

Figure 11 The relationship between the pixel size and the absolute difference of the average values of the refractive index measured by the experimental and estimated patterns.

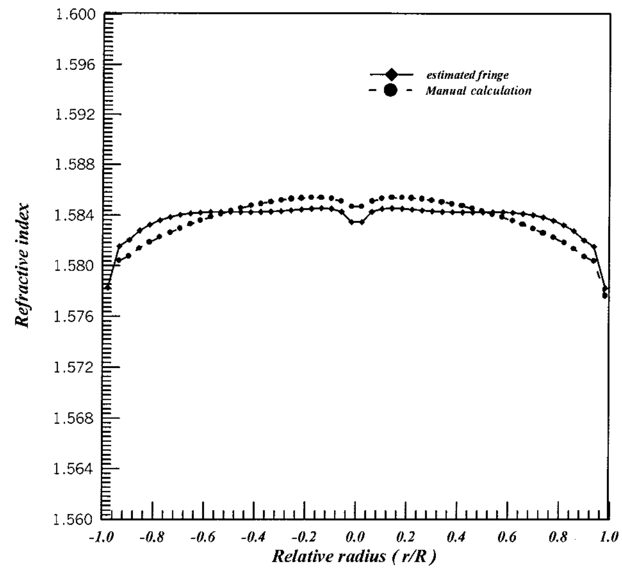

Figure 13 The refractive index profile of the polyethylene fiber with a draw ratio of 7.5 using experimental and estimated patterns. Monochromatic light vibrating parallel to the fiber axis is used. The pixel size is 0.8358 μm, and the immersion liquid has a refractive index of 1.5787.

quality of the interference image being used. The suggested methods described in this article are particularly suitable for applications involving high quality and low quality patterns. On the other hand, we can estimate a new pattern, which coincides with the experimental pattern, and use it to calculate the refractive index profile. The highest accuracy of the refractive index profile was obtained with low pixel size.

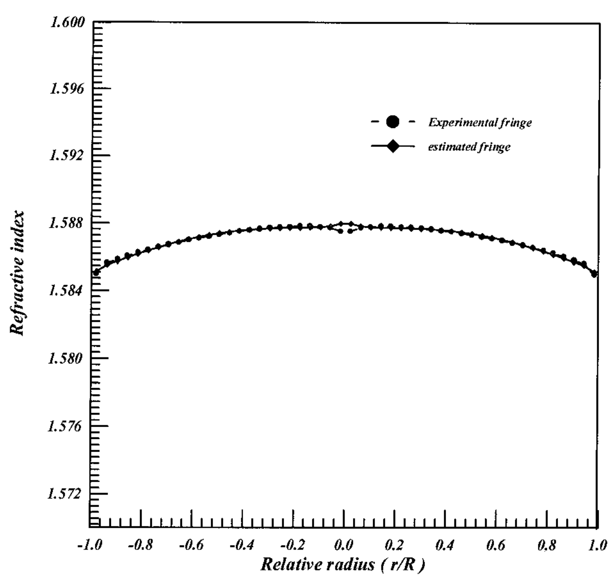

Figure 12 The relationship between the pixel size and the absolute difference of the average values of the refractive index measured by the experimental and estimated patterns. Monochromatic light vibrates parallel to the fiber axis. The pixel size is small enough (0.625 μm), and the immersion liquid has a refractive index of 1.5849.

REFERENCES

1. Zanger, H.; Zanger, C. Fiber Optics Communications and Other Applications; Maxwell Macmillan: New York, 1991.
2. Faust, R. C. Physical Methods of Investigation Textiles; Textile Book Publishers Inc.: New York, 1959.
3. Sounders, M. J.; Gardner, W. B. Appl Opt 1977, 16, 2368.
4. Sochacki, J. Appl Opt 1986, 25, 3473.
5. Hamza, A. A.; Mabrouk, M. A. J Mod Opt 1991, 38, 97.
6. Barakat, N.; Hamza, A. A.; Gonied, A. S. Appl Opt 1985, 24, 4383.
7. Hamza, A. A.; Sokkar, T. Z. N.; Mabrouk, M. A.; Ghandar, A. M.; Ramadan, W. A. Pure Appl Opt 1995, 4, 161.
8. Hamza, A. A.; Sokkar, T. Z. N.; Mabrouk, M. A.; El-Morsy, M. A. J Appl Polym Sci 2000, 77, 3099.
9. Barakat, N.; Hamza, A. A. Interferometry of Fibrous Materials; Adam–Hilger: Bristol, U.K., 1990.

10. Okoski, T. Optical Fibres; Harcourt Brace Jovanovich: New York, 1982.
11. Mabrouk, M. A.; El-Bawab, H. F. Pure Appl Opt 1997, 6, 247.
12. Mabrouk, M. A.; Shams-Eldin, M. A. Pure Appl Opt 1996, 5, 929.
13. Yatagai, T.; Nakadate, S.; Idesawa, M.; Saito, H. Opt Eng 1982, 21, 432.
14. Chen, T. Y.; Taylor, C. E. Exp Mech 1989, 29, 323.
15. Ramesh, K.; Singh, R. K. Electron Imag 1995, 4, 71.
16. Yao, J. Y. Exp Mech 1990, 30, 264.
17. Eichhorn, N.; Osten, W. J Mod Opt 1988, 35, 1717.
18. Yu, Q. Y.; Liu, X. L.; Andresen, K. Appl Opt 1994, 33, 3705.
19. Yu, Q. Y.; Liu, X. L.; Sun, X. Appl Opt 1998, 37, 4504.
20. Takeda, M.; Ina, H.; Kobayashi, S. J Opt Soc Am 1982, 72, 156.
21. Takeda, M.; Mutoh, K. Appl Opt 1983, 22, 3977.
22. Burton, D. R.; Lalor, M. J Proc SPIE 1988, 1010, 17.
23. Bone, D. J. Appl Opt 1991, 30, 3627.
24. Nugent, K. A. Appl Opt 1985, 24, 3101.
25. Lai, G.; Yatagai, T. Appl Opt 1994, 33, 5935.
26. Arevalillo, M.; Burton, D. R.; Lalor, M. J. Opt Laser Engl 1999, 31, 135.
27. Green, R. J.; Walker, J. G.; Robinson, D. W. Opt Laser Engl 1988, 8, 29.
28. Nakadate, S.; Yatagai, T.; Saito, H. Appl Opt 1983, 22, 237.
29. Liu, J. B.; Ronney, P. D. Appl Opt 1997, 36, 6231.